(low Pm), together with the large-scale flow, may be more efficient in transporting magnetic energy to small scales. However, such an effect will vanish in any case when the turbulent eddies become smaller than the length scale l_B at which diffusion dissipates magnetic energy. One interpretation of our finding is that a weak dependence on the magnetic Prandtl number at values $Pm \approx 1$ disappears for $Pm < 1$. We therefore suggest that the simpler scaling law (equation (3)) represents Earth's core conditions reasonably well.

In order to calculate the dissipation of the geodynamo, we must know Rm and the total magnetic energy in the core. We use the dependence of the secular variation on Rm in our dynamo models to estimate the core value. The timescale of secular variation depends on the spherical harmonic degree n, and is defined as:

$$\tau_n = \left[\left\langle \sum_{m=0}^{n} \left(g_{nm}^2 + h_{nm}^2\right) \right\rangle \Big/ \left\langle \sum_{m=0}^{n} \left(\dot{g}_{nm}^2 + \dot{h}_{nm}^2\right) \right\rangle \right]^{1/2}$$

where g,h are the Gauss coefficients, the dot marks their time derivative and $\langle\ \rangle$ the time average. For the geomagnetic field, τ_n decreases with n (ref. 15). To derive a single time constant of secular variation τ_{sec} we attempt a simple fit of the form $\tau_n = \tau_{sec}/n$, although a somewhat stronger dependence on n might better represent the present rate of secular variation (R. Holme, personal communication). Excluding the dipole part, the fit is fair for $n = 2$–8 in the time period 1840–1990 and gives $\tau_{sec} = 535$ yr (Fig. 3a). The secular variation in the dynamo models, averaged over much longer time, follows more closely a $1/n$-dependence. τ_{sec} depends on the inverse of the magnetic Reynolds number (Fig. 3b). The estimated secular variation time of the geomagnetic field requires $Rm = 1{,}200$ in the core, which leads to a magnetic dissipation time of 42 yr.

The factor between the mean magnetic field strength inside the model shell and that in degrees n up to 12 on the outer boundary is in the range of 2.5–5 in our non-reversing dynamos and 7.5 in the reversing case. With a likely factor of 5–7.5 for the geodynamo and an r.m.s. field strength ($n < 13$) at the core–mantle boundary of 0.39 mT (ref. 16), we infer 2–3 mT for the field in the core, which gives $E_{mag} = (2.8\text{–}6.2) \times 10^{20}$ J. From equation (2) the ohmic dissipation is found to be 0.2–0.5 TW.

For the recently preferred high-power-consumption values of the geodynamo of >1 TW (refs 2, 3, 17), the required heating could be supplied by >200 p.p.m. potassium in the core[17]. Although recent experiments suggest that such concentrations are possible[7,18], our result suggesting a more moderate power requirement relaxes severe constraints on core evolution, and removes the strong need for heat sources in the core. The inner core could be much older than 1 Gyr; thermal modelling[1] predicts an inner core age of 2.4 Gyr for $D_{ohm} = 0.5$ TW and ~3.5 Gyr for $D_{ohm} = 0.2$ TW. As the geodynamo must operate differently in the absence of an inner core or may not operate at all, the existence of a magnetic field of roughly present-day strength over the past 3.5 Gyr (ref. 19) is more easily reconciled with an old inner core. □

Received 3 February; accepted 22 March 2004; doi:10.1038/nature02508.

1. Buffett, B. A. Estimates of heat flow in the deep mantle based on the power requirements of the geodynamo. *Geophys. Res. Lett.* **29,** doi:1.1029/2001GL014649 (2002).
2. Roberts, P. H., Jones, C. A. & Calderwood, A. R. in *Earth's Core and Lower Mantle* (eds Jones, C. A., Soward, A. M. & Zhang, K.) 100–129 (Taylor & Francis, London, 2003).
3. Labrosse, S. Thermal and magnetic evolution of the Earth's core. *Phys. Earth Planet. Inter.* **140,** 127–143 (2003).
4. Gubbins, D., Alfè, D., Masters, G., Price, D. & Gillan, M. J. Can the Earth's dynamo run on heat alone? *Geophys. J. Int.* **155,** 609–622 (2003).
5. Nimmo, F., Price, G. D., Brodholt, J. & Gubbins, D. The influence of potassium on core and geodynamo evolution. *Geophys. J. Int.* **156,** 363–376 (2004).
6. Stieglitz, R. & Müller, U. Experimental demonstration of the homogeneous two-scale dynamo. *Phys. Fluids* **13,** 561–564 (2001).
7. Gessmann, C. K. & Wood, B. J. Potassium in the Earth's core? *Earth Planet. Sci. Lett.* **200,** 63–78 (2002).
8. Langel, R. A. & Estes, R. H. A geomagnetic field spectrum. *Geophys. Res. Lett.* **9,** 250–253 (1982).
9. Kuang, W. & Bloxham, J. An Earth-like numerical dynamo model. *Nature* **389,** 371–374 (1997).
10. Roberts, P. H. & Glatzmaier, G. A. A test of the frozen-flux approximation using a new geodynamo model. *Phil. Trans. R. Soc. Lond. A* **358,** 1109–1121 (2000).
11. Christensen, U., Olson, P. & Glatzmaier, G. A. Numerical modeling of the geodynamo: a systematic parameter study. *Geophys. J. Int.* **138,** 393–409 (1999).
12. Kutzner, C. & Christensen, U. R. From stable dipolar to reversing numerical dynamos. *Phys. Earth Planet. Inter.* **131,** 29–45 (2002).
13. Müller, U. & Stieglitz, R. The Karlsruhe dynamo experiment. *Nonlin. Proc. Geophys.* **9,** 165–170 (2002).
14. Tilgner, A. Numerical simulation of the onset of dynamo action in an experimental two-scale dynamo. *Phys. Fluids* **14,** 4092–4094 (2002).
15. Hulot, G. & LeMouël, J. L. A statistical approach to the Earth's main magnetic field. *Phys. Earth Planet. Inter.* **82,** 167–183 (1994).
16. Bloxham, J. & Jackson, A. Time-dependent mapping of the magnetic field at the core-mantle boundary. *J. Geophys. Res.* **97,** 19537–19563 (1992).
17. Buffett, B. A. The thermal state of the Earth's core. *Science* **299,** 1675–1676 (2003).
18. Rama Murthy, V., van Westrenen, W. & Fei, Y. Experimental evidence that potassium is a substantial radioactive heat source in planetary cores. *Nature* **423,** 163–165 (2003).
19. McElhinny, M. W. & Senanayake, W. E. Paleomagnetic evidence for the existence of the geomagnetic field 3.5 Ga ago. *J. Geophys. Res.* **85,** 3523–3528 (1980).
20. Secco, R. A. & Schloessin, H. H. The electrical resistivity of solid and liquid Fe at pressures up to 7 GPa. *J. Geophys. Res.* **94,** 5887–5894 (1989).
21. Bloxham, J., Gubbins, D. & Jackson, A. Geomagnetic secular variations. *Phil. Trans. R. Soc. Lond. A* **329,** 415–502 (1989).

Acknowledgements We thank U. Müller for the permission to use unpublished results from the laboratory dynamo experiment. This work was supported by the priority programme "Geomagnetic secular variations" of the Deutsche Forschungsgemeinschaft.

Competing interests statement The authors declare that they have no competing financial interests.

Correspondence and requests for materials should be addressed to U.R.C. (Christensen@linmpi.mpg.de)

Optimal nitrogen-to-phosphorus stoichiometry of phytoplankton

Christopher A. Klausmeier[1,2], Elena Litchman[2,3], Tanguy Daufresne[1] & Simon A. Levin[1]

[1]*Department of Ecology and Evolutionary Biology, Princeton University, Princeton, New Jersey 08544, USA*
[2]*School of Biology, Georgia Institute of Technology, 310 Ferst Drive, Atlanta, Georgia 30332-0230, USA*
[3]*Institute of Marine and Coastal Sciences, Rutgers University, New Brunswick, New Jersey 08901, USA*

Redfield noted the similarity between the average nitrogen-to-phosphorus ratio in plankton (N:P = 16 by atoms) and in deep oceanic waters (N:P = 15; refs 1, 2). He argued that this was neither a coincidence, nor the result of the plankton adapting to the oceanic stoichiometry, but rather that phytoplankton adjust the N:P stoichiometry of the ocean to meet their requirements through nitrogen fixation, an idea supported by recent modelling studies[3,4]. But what determines the N:P requirements of phytoplankton? Here we use a stoichiometrically explicit model of phytoplankton physiology and resource competition to derive from first principles the optimal phytoplankton stoichiometry under diverse ecological scenarios. Competitive equilibrium favours greater allocation to P-poor resource-acquisition machinery and therefore a higher N:P ratio; exponential growth favours greater allocation to P-rich assembly machinery and therefore a lower N:P ratio. P-limited environments favour slightly less allocation to assembly than N-limited or light-limited environments. The model predicts that optimal N:P ratios will vary from 8.2 to 45.0, depending on the ecological conditions. Our results show that the canonical Redfield N:P ratio of 16 is not a universal biochemical optimum, but instead represents an average of species-specific N:P ratios.

Laboratory studies show that phytoplankton are flexible in their overall stoichiometry, often matching their nutrient supply at low growth rates[5–7]. However, this variability is largely due to stored nutrients: underneath these variable pools is the relatively constant composition of the cells' functional machinery[6]. This structural stoichiometry determines the nutrient requirements of the species. Physiological studies have shown that the structural N:P ratio is species-specific[8]. Figure 1 shows the structural N:P ratios of 29 freshwater and marine species (see Supplementary Information). Although the median structural N:P of 17.7 is close to the Redfield ratio, structural N:P ratios range from 7.1 to 43.3, with an outlier at 133.3. Although this data set does not include the structural N:P ratios of the abundant marine picoplankton, *Synechococcus* and *Prochlorococcus*, recent studies[9,10] have shown that their N:P ratios during exponential growth range from 13.3 to 33.2 and 15.9 to 24.4 respectively, within the range of our data set. We aim to understand the causes of and limits to this interspecific variation, building on recent work on the chemical composition of cellular machinery[11,12].

Our approach to deriving optimal phytoplankton stoichiometry has three steps. First, we analyse an underlying model of a single species of phytoplankton given its structural stoichiometry and ecological parameters. Next, we characterize a species by its allocation to two broad classes of cellular machinery: assembly machinery and resource-acquisition machinery. Assembly machinery corresponds to ribosomes, which contain both N and P, and resource-acquisition machinery corresponds to nutrient-uptake proteins and chloroplasts, which contain N but little or no P (refs 6, 12). The allocation strategy determines both the ecological parameters and the structural stoichiometry. We follow the growth-rate hypothesis, that ribosome/RNA content largely explains both the growth rate and the P content of organisms[6]. Finally, we determine the optimal strategy under opposite ecological scenarios: during exponential growth and at competitive equilibrium under different limiting resources (N, P and light). Others have modelled carbon allocation to different cellular components[13,14], but these physiological models do not investigate N:P ratios or use competition theory to determine the optimal allocation patterns under diverse ecological conditions.

During exponential growth at saturating resource levels, the optimal strategy maximizes the growth rate, μ_{max} (Fig. 2a). Using the parameters given below (see Methods), we find the optimal allocation-to-assembly under exponential growth, $R_a = 0.645$, giving a structural N:P ratio of 8.2. At competitive equilibrium, the optimal strategy minimizes the break-even requirement of the limiting resource, R^* (Fig. 2b–d, ref. 15). The optimal allocation strategy depends on which resource is limiting: (1) under light limitation, the optimal allocation-to-assembly is $R_a = 0.0447$, giving a structural N:P ratio of 35.8; (2) under N limitation, the optimal strategy is $R_a = 0.0388$, giving a structural N:P ratio of 37.4; and (3) under P limitation, the optimal strategy is $R_a = 0.0164$, giving a structural N:P ratio of 45.0. Colimitation results in an optimal strategy between these values that depends on the resource supply ratio. These optimal N:P ratios roughly bracket the range of variation observed in different species (Fig. 1). The optimal strategy at equilibrium depends on the mortality rate the phytoplankton experience; so conditions of high mortality, such as during intense grazing, lead to greater allocation to assembly-machinery and therefore a lower N:P ratio. In all cases, the optimal strategy balances the conflicting needs for resource acquisition and cellular assembly. Although our parameterization is necessarily rough, given the available data, our qualitative conclusion that the ecological trade-off between rapid growth and equilibrium competitive ability generates a range of optimal N:P ratios is robust to variation in model parameters.

Nitrogen-fixing species often have a higher N:P stoichiometry than non-fixing species. For example, *Trichodesmium* blooms have N:P ratios ranging from 42 to 125 (ref. 16). A simple explanation for N-fixers' high N:P ratios is that they have an exclusive and inexhaustible N supply. Our model suggests another, less obvious explanation. N fixation is energetically costly, leading to a lower v_I' in our model (less carbon incorporated per unit light energy absorbed; see Methods), as observed for *Trichodesmium*[16]. Decreasing v_I' increases allocation to light harvesting and decreases allocation to assembly machinery. Therefore, by this mechanism, N fixers have high N:P ratios because they need more light-harvesting machinery to power N fixation at the expense of P-rich assembly machinery. Because both ribosomes and choloroplasts are N-rich, the high N:P ratio of N fixers is mainly due to a low minimum P quota $Q_{min,P}$.

In our model, for a given environment a single strategy is optimal and displaces all others. Therefore, our approach does not address Hutchinson's paradox of plankton diversity[17]. However,

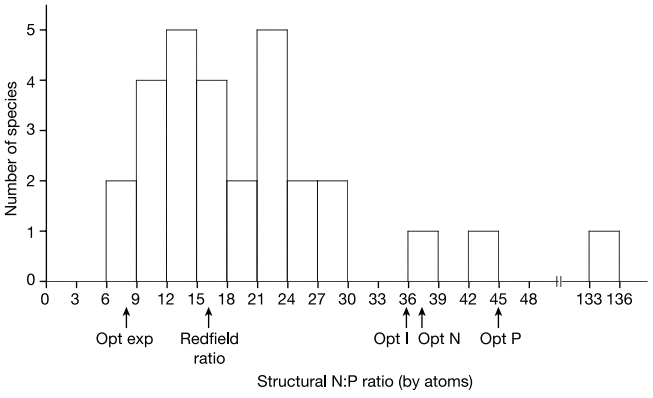

Figure 1 Structural N:P ratio of 29 species of freshwater and marine phytoplankton. The Redfield ratio is shown, as is the theoretical range predicted by the model under the extreme ecological conditions of exponential growth (Opt exp) and competitive equilibrium with light, N and P limiting (Opt I, Opt N and Opt P) conditions.

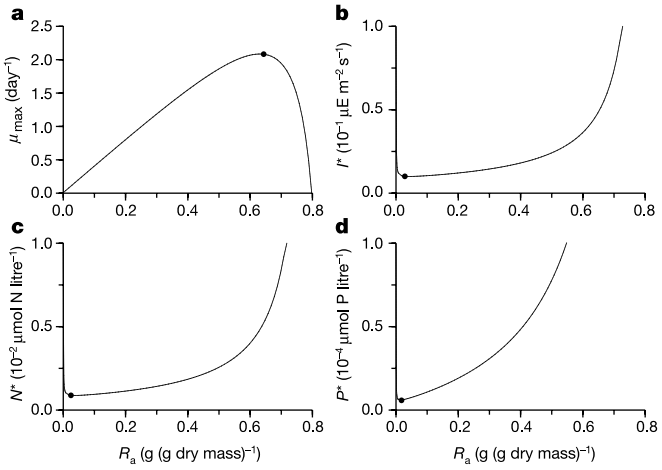

Figure 2 Fitness measures as a function of allocation to assembly machinery. **a**, Maximum growth rate, μ_{max}, **b**–**d**, break-even light (**b**), N (**c**) and (**d**) P levels. Species with low R^* values are good equilibrium competitors while those with high μ_{max} values are favoured under conditions of exponential growth. The optimal strategies are marked with dots. Note that the allocation to assembly is much higher under exponential growth (**a**) than at competitive equilibrium (**b**–**d**), and slightly higher under light and N limitation (**b**, **c**) than under P limitation (**d**). Half-saturation constants used: $K_I = 50\,\mu E\,m^{-2}\,s^{-1}$, $K_N = 5.6\,\mu mol\ N\ litre^{-1}$, and $K_P = 0.2\,\mu mol\ P\ litre^{-1}$, but these merely scale the graphs in **b**–**d**.

many mechanisms of coexistence have been explored[18], effectively resolving Hutchinson's paradox. It may be useful to extend our approach to models that permit multispecies coexistence.

The strategic perspective that we take in our model does not specify the level at which variation in allocation occurs. Although species vary in their structural stoichiometries (Fig. 1), intraspecific variation is also possible, owing to either genetic diversity or physiological flexibility. For example, in a series of chemostat growth experiments with a single species, as the dilution rate passed a critical value, the physiological parameters of the culture changed dramatically[19]. The 'slow-adapted' cells grown at low-dilution rates had an asymptotic growth rate, μ, of 0.536 day^{-1} and $Q_{\min,P} = 9 \times 10^{-17}$ mol P cell^{-1}, while the 'fast-adapted' cells had $\mu = 1.13$ day^{-1} and $Q_{\min,P} = 3.61 \times 10^{-16}$ mol P cell^{-1}. This agrees with our model, which predicts greater allocation to ribosomes and therefore increased P content at high mortality/growth rates.

The Redfield N:P ratio of 16 does not emerge as a universally optimal value from either our empirical survey (Fig. 1) or our theoretical results. Instead, it should be seen as merely the current average stoichiometry of phytoplankton in the ocean, weighted by the relative abundance of species with different structural N:P ratios. In turn, the relative abundance of species is determined by the ecological conditions under which species grow and compete. Competitive equilibrium selects high N:P ratios; exponential growth selects low N:P ratios. Real ecosystems experience a mix of equilibrium and exponential growth phases[20], and therefore select species with intermediate N:P ratios (C.A.K., unpublished results). The major determinants of the optimal stoichiometry are the biology and stoichiometry of ribosomes and proteins and the mixture of exponential growth and equilibrium phases; the identity of the limiting resource plays a minor role (Fig. 1). Most of the variation in the optimal N:P ratio in our model results from variation in $Q_{\min,P}$, because all types of machinery contain similar amounts of N.

An implication of this view is that N:P ratios in the ocean could vary over time, simply because of changes in the ecological balance between exponential growth and equilibrium phases, or in N and P availability. Falkowski[2] asked whether biologists could rule out Broecker and Henderson's hypothesis that N:P ratios rose to 25 during glacial periods[21]. Our results show that this ratio is possible and provide a mechanism that would allow decadal variation in N:P ratios, as has been recently suggested[22]. Although our model explains structural stoichiometry, the overall stoichiometry (structures plus stores) matches structural stoichiometry during exponential growth[7], and structural stoichiometry defines the N:P requirements of phytoplankton that diazotrophs match through N-fixation. At equilibrium at low mortality/growth rates, the overall N:P stoichiometry is close to the N:P supply ratio[6,7].

We suggest that field surveys[23] should focus less on average values and more on the variation in particulate and dissolved nutrient ratios, by using higher spatial and temporal resolution and presenting the range of values observed rather than just averages. An analysis of long-term time-series data from the North Pacific illustrates the significant temporal variability in N:P stoichiometry[24]. We await a simiarly extensive study of spatial variability in N:P ratios in the sea. Although deep-water stoichiometry integrates over long-time and whole-basin scales and should be relatively constant in time and space, we suspect that greater variability may exist in surface particulate ratios than has been thought, as has been recently documented for C:N ratios[25].

We have focused on understanding N:P ratios because N and P are major macroelements in phytoplankton, possibly limiting their growth, and playing an important part in coupled biogeochemical cycles. A recent study has extended the concept of the Redfield-ratio to include trace elements[26]. Different cellular components may be involved, but we believe that our general modelling approach linking cellular allocation patterns with competitive ability under different ecological conditions could yield insights into the basis of these other elemental ratios. This approach could also be extended to other ecological trade-offs by considering the different types of cellular machinery. □

Methods

Model and analysis

We use a three-resource version of Droop's model for phytoplankton growth, with equations for cell density, B, and the resource (R) to cell quotas, Q_R. The quota includes both structural and storage pools. Quotas increase with nutrient uptake or photosynthesis, modelled using a Michaelis–Menten function, $f_R(R) = v_R R/(K_R + R)$, where K is the half-saturation constant, and decrease with growth, which is taken to be the minimum of three Droop functions[7,19]. The growth rate at infinite quota is μ, and $Q_{\min,R}$ is the minimum quota at which growth ceases, corresponding to the amount of this element in the cell's structural machinery. Cell density increases with growth and decreases with density-independent mortality.

$$\begin{aligned}
\frac{dQ_P}{dt} &= f_P(P) - \mu \min\left(1 - \frac{Q_{\min,P}}{Q_P}, 1 - \frac{Q_{\min,N}}{Q_N}, 1 - \frac{Q_{\min,C}}{Q_C}\right) Q_P \\
\frac{dQ_N}{dt} &= f_N(N) - \mu \min\left(1 - \frac{Q_{\min,P}}{Q_P}, 1 - \frac{Q_{\min,N}}{Q_N}, 1 - \frac{Q_{\min,C}}{Q_C}\right) Q_N \\
\frac{dQ_C}{dt} &= f_I(I) - \mu \min\left(1 - \frac{Q_{\min,P}}{Q_P}, 1 - \frac{Q_{\min,N}}{Q_N}, 1 - \frac{Q_{\min,C}}{Q_C}\right) Q_C \\
\frac{dB}{dt} &= \mu \min\left(1 - \frac{Q_{\min,P}}{Q_P}, 1 - \frac{Q_{\min,N}}{Q_N}, 1 - \frac{Q_{\min,C}}{Q_C}\right) B - mB
\end{aligned} \tag{1}$$

where P, N and I are the available P, N and light levels and m is the mortality rate. These equations are typically supplemented with equations describing the resource dynamics, but because our results do not depend on the exact form of the resource equations, we omit them. Each species follows a set of equations as in (1), and species compete solely through shared use of the resources.

As in general resource–consumer models[15], a species' equilibrium competitive ability for each resource is summarized by the break-even resource level, R^*. For this model[7]:

$$\begin{aligned}
P^* &= \frac{m\mu K_P Q_{\min,P}}{v_P(\mu - m) - m\mu Q_{\min,P}} \\
N^* &= \frac{m\mu K_N Q_{\min,N}}{v_N(\mu - m) - m\mu Q_{\min,N}} \\
I^* &= \frac{m\mu K_I Q_{\min,C}}{v_I(\mu - m) - m\mu Q_{\min,C}}
\end{aligned} \tag{2}$$

(P^*, N^*, I^*) is the corner of an L-shaped zero-net-growth-isocline (ZNGI) typical of essential resources[15]. Phytoplankton can grow when $P > P^*$, $N > N^*$ and $I > I^*$, that is, when resource levels are above the ZNGI, and at equilibrium draw the resources down to some point on the ZNGI. The maximum growth rate realised when a population grows exponentially in a resource-saturated habitat is:

$$\mu_{\max} = \min\left(\frac{\mu v_P}{\mu Q_{\min,P} + v_P}, \frac{\mu v_N}{\mu Q_{\min,N} + v_N}, \frac{\mu v_I}{\mu Q_{\min,C} + v_I}\right) \tag{3}$$

assuming that the quota equilibrates quickly[7].

We characterize a species by its allocation to four different kinds of cellular machinery: assembly machinery (ribosomes) and three types of resource-acquisition machinery (N- and P-uptake proteins and chloroplasts). These make up R_a, R_N, R_P and R_I proportions of dry mass, respectively. Each type of machinery has its own chemical composition, with N_x the proportion of N and P_x the proportion of P. We assume that these types of machinery constitute a fixed proportion p of the cell's dry mass, which provides a trade-off between the different components.

$$R_a + R_N + R_P + R_I = p \tag{4}$$

The $1 - p$ proportion of biomass that we do not actively consider is assigned its own stoichiometry, (N_o, P_o). The allocation strategy determines the species' maximum assembly rate and resource uptake rates:

$$\mu = \mu' R_a, v_N = v_N' R_N, v_P = v_P' R_P, v_I = v_I' R_I \tag{5}$$

where the primed parameters quantify the efficiency of each kind of machinery. The allocation strategy also determines the N and P content in structural material:

$$\begin{aligned}
Q_{\min,N} &= w(R_a N_a + R_N N_N + R_P N_P + R_I N_I + (1 - p)N_o) \\
Q_{\min,P} &= w(R_a P_a + R_N P_N + R_P P_P + R_I P_I + (1 - p)P_o)
\end{aligned} \tag{6}$$

where w is cell weight (g dry mass cell^{-1}). The structural N:P ratio is $Q_{\min,N}/Q_{\min,P}$. Together, equations (4)–(6) map the physiological allocation strategy into ecological parameters and structural stoichiometry.

Substituting equations (4)–(6) into equation (3), we find $\mu_{\max}$ as a function of R_a (Fig. 2a). The optimal strategy during exponential growth maximizes $\mu_{\max}$. Substituting equations (4)–(6) into equation (2), we get a formula for R^* for each resource as a function of allocation to assembly machinery (Fig. 2b–d). We find the optimal strategy at equilibrium by minimizing R^* for each resource. Algebraic expressions for the optimal strategies are unwieldy, but can easily be found numerically.

Parameterization

The proportion of cell dry mass allocated to assembly and uptake machinery is set at $p = 0.8$, from the upper-end of the range (0.33–0.8) of protein + RNA (ref. 12). Chemical composition: assembly machinery (ribosomes), $N_a = 0.162$, $P_a = 0.053$; nutrient-uptake

machinery (proteins), $N_N = N_P = 0.17$, $P_N = P_P = 0$; light-harvesting machinery (chloroplasts), $N_I = 0.113$ and $P_I = 0.0032$ (ref. 6). As a neutral choice, we set the composition of the other biomass to the Redfield ratio, $N_o = 0.0631$, $P_o = 0.00873$; our results are relatively insensitive to these values. Assembly-machinery efficiency was set to $\mu' = 4.0\,\mathrm{day}^{-1}\,(\mathrm{g\,(g\,dry\,mass)}^{-1})^{-1}$ (ref. 13). Maximum carbon-uptake efficiency was set to $v'_I = w\,(16.8\,\mathrm{g\,C\,day}^{-1}\,\mathrm{g}^{-1})$, using $P^b_{\mathrm{opt}} = 20\,\mathrm{mg\,C\,hr}^{-1}\,(\mathrm{mg\ chl}\ a)^{-1}$ (ref. 27), where superscript b indicates normalization to biomass, and the proportion of chlorophyll a in chloroplasts being 0.035 (ref. 28). Maximum N- and P-uptake efficiencies were set to $v'_N = w\,(3.0 \times 10^3\,\mathrm{g\,N\,day}^{-1}\,(\mathrm{g\ N\text{-}uptake\ protein})^{-1})$ and $v'_P = w\,(6.7 \times 10^3\,\mathrm{g\,P\,day}^{-1}\,(\mathrm{g\ P\text{-}uptake\ protein})^{-1})$, based on nutrient-transporter turnover times of 0.01 s (refs 29, 30). The minimum carbon quota was set to $Q_{\mathrm{min},C} = 0.24w$ (ref. 12). The results are independent of cell weight because w cancels from the expression for optimal R_a. The mortality rate was set to $m = 0.01\,\mathrm{day}^{-1}$, chosen from the low end of the observed range to illustrate the lowest feasible value of allocation to assembly machinery. We fix the ratio of uptake machinery types to achieve colimitation during exponential growth, by equating the three terms in the minimum of equation (3). This results in $R_N = 0.00317\,R_u$, $R_P = 0.000381\,R_u$, and $R_I = 0.996\,R_u$, which agrees with the observation that nutrient-uptake proteins are usually a much smaller component of biomass than chloroplasts.

Received 31 December 2003; accepted 27 February 2004; doi:10.1038/nature02454.

1. Redfield, A. C. The biological control of chemical factors in the environment. *Am. Sci.* **46,** 205–221 (1958).
2. Falkowski, P. G. Rationalizing elemental ratios in unicellular algae. *J. Phycol.* **36,** 3–6 (2000).
3. Tyrrell, T. The relative influences of nitrogen and phosphorus on oceanic primary production. *Nature* **400,** 525–531 (1999).
4. Lenton, T. M. & Watson, A. J. Redfield revisited 1. Regulation of nitrate, phosphate, and oxygen in the ocean. *Glob. Biogeochem. Cycles* **14,** 225–248 (2001).
5. Rhee, G.-Y. Effects of N:P atomic ratios and nitrate limitation on algal growth, cell composition and nitrate uptake. *Limnol. Oceanogr.* **23,** 10–25 (1978).
6. Sterner, R. W. & Elser, J. J. *Ecological Stoichiometry: The Biology of Elements from Molecules to the Biosphere* (Princeton Univ. Press, Princeton, 2002).
7. Klausmeier, C. A., Litchman, E. & Levin, S. A. Phytoplankton growth and stoichiometry under multiple nutrient limitation. *Limnol. Oceanogr.* (in the press).
8. Rhee, G.-Y. & Gotham, I. J. Optimum N:P ratios and coexistence of planktonic algae. *J. Phycol.* **16,** 486–489 (1980).
9. Bertilsson, S., Berglund, O., Karl, D. M. & Chisholm, S. W. Elemental composition of marine *Prochlorococcus* and *Synechococcus*: implications for the ecological stoichiometry of the sea. *Limnol. Oceanogr.* **48,** 1721–1731 (2003).
10. Heldal, M., Scanlan, D. J., Norland, S., Thingstad, F. & Mann, N. H. Elemental composition of single cells of various strains of marine *Prochlorococcus Synechococcus* using X-ray microanalysis. *Limnol. Oceanogr.* **47,** 1732–1743 (2003).
11. Elser, J. J., Dobberfuhl, D., MacKay, N. A. & Schampel, J. H. Organism size, life history, and N:P stoichiometry: towards a unified view of cellular and ecosystem processes. *BioScience* **46,** 674–684 (1996).
12. Geider, R. J. & LaRoche, J. Redfield revisited: variability of C:N:P in marine microalgae and its biochemical basis. *Eur. J. Phycol.* **37,** 1–17 (2002).
13. Shuter, B. J. A model of physiological adaptation in unicellular algae. *J. Theor. Biol.* **78,** 519–552 (1979).
14. Kooijman, S. A. L. M. *Dynamic Energy and Mass Budgets in Biological Systems* 2nd edn (Cambridge Univ. Press, UK, 2000).
15. Tilman, D. *Resource Competition and Community Structure* (Princeton Univ. Press, NJ, 1982).
16. Letelier, R. M. & Karl, D. M. Role of *Trichodesmium* spp. in the productivity of the subtropical North Pacific Ocean. *Mar. Ecol. Prog. Ser.* **133,** 263–273 (1996).
17. Hutchinson, G. E. The paradox of the plankton. *Am. Nat.* **95,** 137–145 (1961).
18. Tilman, D. & Pacala, S. in *Species Diversity in Ecological Communities* (eds Ricklets, R. & Schluter, D.) 13–25 (Univ. Chicago Press, Chicago, 1993).
19. Droop, M. R. The nutrient status of algal cells in continuous culture. *J. Mar. Biol. Assoc. UK* **54,** 825–855 (1974).
20. Litchman, E. & Klausmeier, C. A. Competition of phytoplankton under fluctuating light. *Am. Nat.* **157,** 170–187 (2001).
21. Broecker, W. S. & Henderson, G. M. The sequence of events surrounding Termination II and their implications for the cause of glacial-interglacial CO_2 changes. *Paleoceanogr.* **13,** 352–364 (1998).
22. Pahlow, M. & Riebesell, U. Temporal trends in deep ocean Redfield ratios. *Science* **287,** 831–833 (2001).
23. Copin-Montegut, C. & Copin-Montegut, G. Stoichiometry of carbon, nitrogen, and phosphorus in marine particulate matter. *Deep-Sea Res.* **30,** 31–46 (1983).
24. Karl, D. M. *et al.* Ecological nitrogen-to-phosphorus stoichiometry at station ALOHA. *Deep-Sea Res. II* **48,** 1529–1566 (2001).
25. Schneider, B., Schlitzer, R., Fischer, G. & Nöthig, E.-M. Depth-dependent elemental compositions of particulate organic matter (POM) in the ocean. *Glob. Biogeochem. Cycles* **17,** 1032 (2003).
26. Quigg, A. *et al.* The evolutionary inheritance of elemental stoichiometry in marine phytoplankton. *Nature* **425,** 291–294 (2003).
27. Behrenfeld, M. J. & Falkowski, P. G. A consumer's guide to phytoplankton primary productivity models. *Limnol. Oceanogr.* **42,** 1479–1491 (1997).
28. Kirk, J. T. O. & Tilney-Bassett, R. A. E. *The Plastids: Their Chemistry, Structure, Growth and Inheritance* 6 (Freeman Press, London, 1967).
29. Raven, J. A. Nutrient transport in microalgae. *Ad. Microb. Physiol.* **21,** 147–226 (1980).
30. Aksnes, D. L. & Egge, J. K. A theoretical model for nutrient uptake in phytoplankton. *Mar. Ecol. Prog. Ser.* **70,** 65–72 (1991).

Supplementary Information accompanies the paper on **www.nature.com/nature**.

Acknowledgements We thank P. Falkowski, I. Loladze, S. Pacala and D. Tilman for comments and discussion. We acknowledge support from the Andrew W. Mellon Foundation and the National Science Foundation.

Competing interests statement The authors declare that they have no competing financial interests.

Correspondence and requests for materials should be addressed to C.A.K. (christopher.klausmeier@biology.gatech.edu).

Food-web interactions govern the resistance of communities after non-random extinctions

Anthony R. Ives & Bradley J. Cardinale

Department of Zoology, UW-Madison, Madison, Wisconsin 53706, USA

Growing concern about how loss of biodiversity will affect ecosystems has stimulated numerous studies[1–5]. Although most studies have assumed that species go extinct randomly[6–8], species often go extinct in order of their sensitivity to a stress that intensifies through time (such as climate change)[9]. Here we show that the consequences of random and ordered extinctions differ. Both depend on food-web interactions that create compensation; that is, the increase of some species when their competitors and/or predators decrease in density due to environmental stress. Compensation makes communities as a whole more resistant to stress by reducing changes in combined species densities. As extinctions progress, the potential for compensation is depleted, and communities become progressively less resistant. For ordered extinctions, however, this depletion is offset and communities retain their resistance, because the surviving species have greater average resistance to the stress. Despite extinctions being ordered, changes in the food web with successive extinctions make it difficult to predict which species will show compensation in the future. This unpredictability argues for 'whole-ecosystem' approaches to biodiversity conservation, as seemingly insignificant species may become important after other species go extinct.

Interactions among species make it difficult to predict how ecological communities will respond to environmental degradation[10], for two reasons. First, the sensitivity of an individual species to environmental degradation depends not only on the direct impact of degradation on that species, but also on the indirect effects on that species caused by changes in densities of other species[11–13]. For example, environmental degradation may decrease the density of competitors and/or predators of a species, thereby causing a compensatory increase in the density of that species[14–17]. Second, as species go extinct, links within the food web are severed, changing the pathways through which indirect effects operate. Changes in food-web structure depend on the order in which species go extinct, making it difficult to extrapolate from studies that assume extinctions are random to real communities facing progressively intensifying stress from environmental degradation[18].

To disentangle the effects of species interactions on the ability of communities to tolerate environmental degradation, we used mathematical simulations to compare how communities resist changes in abundance as species go extinct randomly versus going extinct in order of their sensitivity to an environmental stress. We